Korean J. Chem. Eng., **22**(6), 822-829 (2005)

Run-to-Run Control of Inductively Coupled C_2F_6 Plasma Etching of SiO_2: Construction of a Numerical Process with a Computational Fluid Dynamics Code

Seung Taek Seo, Yong Hee Lee*, Kwang Soon Lee†, Bum Kyoo Choi* and Dae Rook Yang****

Department of Chemical and Biomolecular Eng.,
*Department of Mechanical Eng., Sogang University, 1-Shinsoodong, Mapogu, Seoul 121-742, Korea
**Department of Chemical and Biomolecular Eng., Korea University, 1-Anamdong, Seongbukgu, Seoul 136-701, Korea
***Currently, with LSI Division of Samsung Electronics Co., 446-711, Korea
(*Received 13 May 2005 • accepted 21 June 2005*)

Abstract−A numerical process to simulate SiO_2 dry etching with inductively coupled C_2F_6 plasmas has been constructed using a commercial CFD code as a first step to design a run-to-run control system. The simulator was found to reasonably predict the reactive ion etching behavior of C_2F_6 plasmas and used to investigate the effects of plasma operating variables on the etch rate and uniformity. The relationship between the operating variables and the etching characteristics was mathematically modeled through linear regression for future run-to-run control system design.

Key words: ICP Etcher, C_2F_6 Plasmas, SiO_2 Etching, Run-to-Run Control

INTRODUCTION

Plasma processing plays an important role in micro-electronics fabrication. In recent semi-conductor fabs, around one-third of the manufacturing steps are known to be related to the plasma processing such as dry etching, chemical vapor deposition, cleaning, and ashing. Among them, dry etching is regarded as the trickiest application because of the complicated and poorly understood surface reactions. For this reason, the operating conditions for plasma etchers are usually found through time-consuming trial-and-error test runs. Such a difficulty may be overcome if we have a systematic and efficient way to search for the optimum operating condition. With the above problem in mind, a research to develop a run-to-run control technique has been conducted for SiO_2 film etching with C_2F_6 inductively coupled plasma (ICP).

The ICP is generated by an RF current passing through a coil winding around a dielectric chamber. The RF current produces a magnetic field changing in upward and downward directions, which induces a circular electric field along which the electrons move while colliding with other gas particles in the chamber. This significantly extends the lifetime of electrons before they annihilate by neutralization on the chamber wall, and makes it possible to achieve higher density plasma than in the capacitively coupled plasma. Another advantage of the ICP etcher is that a separate RF power can be applied to the wafer chuck. The RF power develops a bias potential over the sheath through which ions are accelerated and bombard the wafer surface. In this way, the ion bombardment energy can be independently controlled by the chuck RF power while the plasma density can be adjusted by the chamber RF power [Lieberman and Lichtenberg, 1994].

In SiO_2 etching, fluorocarbon plasmas are widely used due to the high etch rate and selectivity over Si etching [Bell et al., 1994; Oehrlein et al., 1994; An et al., 1999; Rolland et al., 2000; Xiao, 2001]. The fluorocarbon gas can be chosen among CF_4, C_2F_6, and possibly other higher carbon content gases. By the collision with high energy electrons, the gas is dissociated into different radicals and ions like F, CF_x, and CF_x^+. In typical ICP, less than a few percent of the feed gas is dissociated into the plasma components. It is known that the CF_x radicals tend to attach to the SiO_2 surface producing active monomer sites. The active monomer sites are turned to active polymer sites by combining again with incoming CF_x radicals. These sites continue to grow and form passivation polymer layers, whose F/C ratio is about one, on the SiO_2 surface [Thomas et al., 1986; Booth et al., 1989; Tserepi et al., 1997]. On the other hand, the ions attack the SiO_2 surface and the passivation layer with high bombardment energy and etch the surface through reaction or by sputtering. Hence, two competitive reactions, polymer layer forming and etching, take place on the SiO_2 surface at the same time. Which one dominates the other mainly depends on the ion bombardment energy and the F/C ratio of the feed gas. Fig. 1 shows an exemplary operating window for etching versus polymerization. For high bias voltage, *i.e.*, large ion bombardment energy, and high

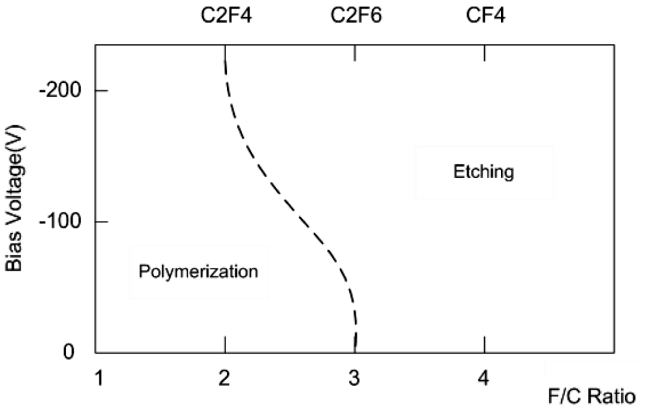

Fig. 1. Typical operating window for polymerization and etching in SiO_2 etching [Xiao, 2001].

†To whom correspondence should be addressed.
E-mail: kslee@sogang.ac.kr

F/C gases, etching governs the surface reaction, and vice versa.

In SiO_2 etching, atomic or molecular oxygen is produced when fluorine radical reacts with SiO_2. The oxygen is apt to react with CF_x radicals to form CO and CO_2, and consequently, suppresses the polymerization. In Si etching, however, no oxygen comes out and the polymer layer forming is not hindered by carbon depletion. This is why fluorocarbon gases can have higher etching selectivity on SiO_2 than Si.

In plasma etching, the etch rate and uniformity are the two most important quality variables. They depend on ion flux and energy as well as neutral radical flux [Gray et al., 1993]. Among them, the ion energy can be manipulated by adjusting the bias voltage or equivalently, the RF power applied to the wafer chuck, whereas the ion and neutral fluxes are complex functions of chamber pressure, RF power, and gas flow rate. Therefore, determination of the operating variables for a desired etching state usually becomes a nontrivial task.

In this research, a numerical simulator has been developed for an ICP etcher for SiO_2 etching with C_2F_6 plasmas using a commercial CFD code called CFD-ACE+/TOPO with the final goal to develop a run-to-run control system of the etcher. The simulator can be used as a test plant as well as an underlying model from which the run-to-run controller is derived. The controller can be employed to improve the operation of real processes since run-to-run control is able to accommodate model uncertainty of roughly up to 100% without losing its ultimate performance [Kim et al., 2000]. To develop the simulator, we judiciously tuned the associated simulation modules in CFD-ACE+/TOPO by selecting appropriate reaction sets and adjusting kinetic parameters for the gas phase as well as surface reactions. With the simulator, the effects of operating variables including RF power, bias voltage, and chamber pressure on the etch rate and uniformity were investigated. Finally, a linear input-output model was derived for future run-to-run controller design.

ICP ETCHER MODEL BY CFD-ACE+

1. Process Description

A schematic diagram of the ICP etcher concerned in this study is given in Fig. 2. It has a multi-turn RF coil around the dielectric plasma chamber. The 13.56 MHz RF power is inductively coupled to the plasma by transformer action and the plasma acts as a single-turn lossy conductor. To the wafer chuck, a separate 13.56 MHz RF source is connected for independent adjustment of ion bombardment. The wafer temperature is controlled by a gas cooling system. The etcher has an axisymmetric shape and a 2-dimensinal model was considered to represent the process. In fact, the etcher model considered in this sturdy is a simplified model of the Multiplex plasma etcher from Surface Technology System Co.

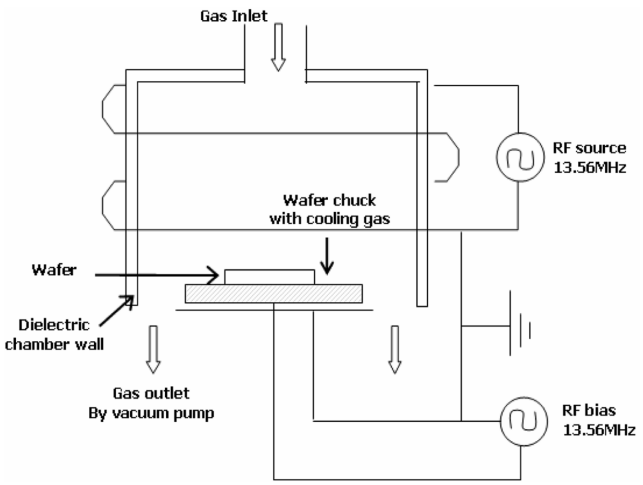

Fig. 2. Schematic diagram of the ICP etcher.

2. Governing Equations

The governing equations for the ICP etcher consist of mass, momentum, and enthalpy balances with appropriate boundary conditions for ionic and neutral species and also for electrons that comprise the plasmas. The balance equations are completed by necessary constitutive equations such as reaction equations in the bulk plasma as well as on the wafer surface, electro-magnetic relationships, thermodynamic and transport relationships, and so forth. In reality, rigorous description of all the above equations is formidable and solving them as a whole is impractical. Hence, simplification to a reasonable degree is necessary.

In the ICP etcher model in CFD-ACE+, neutrals, ions, and electrons are treated in different ways according to their unique characteristics. For neutrals consisting of gas molecules and radicals, mass and momentum balances for usual uncharged fluids are considered for each component. For ions, external force by the electric field is included in the momentum balance. In addition, the flux density in the mass balance is described for each component i by the following drift diffusion approximation:

$$\mathbf{J}_i = -\rho D_i \nabla y_i + \rho y_i \mathbf{u}_{di} + \mathbf{J}_c \tag{1}$$

where y, ρ, and D denote the mass fraction, mass density, and diffusion coefficient, respectively; $\mathbf{u}_d$ is the drift velocity given by

$$\mathbf{u}_{di} = \mathbf{E}(q_i \mu_i - \sum_j q_j \mu_j y_j) \tag{2}$$

where $\mathbf{E}$, q, and μ are electric field, charge, and mobility, respectively. $\mathbf{J}_c$ represents a bulk mass flux that appears to satisfy the mass conservation $\sum \mathbf{J}_i = 0$. The temperature of ions and neutrals is assumed to be same and described by a single enthalpy balance equation. In the enthalpy balance, Joule heating (or Ohmic heating) by the ion current in the electric field is considered together with the heat of reaction (energy gain or loss by collisions).

For electrons, the number density is obtained from that of ions by the quasi-neutrality condition instead of solving the mass balance equation. Also the electron flux density is calculated by the following drift diffusion approximation instead of the solving the momentum balance equation:

$$\mathbf{J}_e = \mu_e n_e \mathbf{E} - D_e \nabla n_e \tag{3}$$

where n_e denotes the number density of electron. The energy balance is written in terms of the electron temperature T_e such that

$$\frac{3}{2}\frac{\partial}{\partial t}(n_e T_e) + \nabla \cdot \left(\frac{5}{2} T_e \mathbf{J}_e - \frac{5}{2} n_e D_e \nabla T_e\right) = -\mathbf{J}_e \cdot \mathbf{E} + P_{ext} - L \tag{4}$$

In the above, the energy flux consists of a convection term $(5/2)T_e\mathbf{J}_e$ and thermo-diffusion term $(5/2)n_eD_e\nabla T_e$. $-\mathbf{J}_e \cdot \mathbf{E}$, P_{ext}, and L represent the joule heating absorbed by electrons, the collisionless heating, and the energy loss by reactions, respectively.

In CFD-ACE+, the mass balance for the gas molecules and the momentum balances for the ions and neutrals are solved in the flow module; the mass balances for the ions and radicals are solved in the chemistry module; the enthalpy balances for the ions and neutrals are solved in the heat transfer module; and the enthalpy balance for the electron and the electron number density from the quasi-neutrality condition are solved in the plasma module. The plasma module also provides plasma specific constitutive terms required by other modules. The electric field is computed in the electric and magnetic modules according to

$$\mathbf{E} = -\nabla\varphi - \frac{\partial \mathbf{A}}{\partial t} \tag{5}$$

where φ and **A** denote the electrostatic and vector magnetic potentials, respectively, which are obtained by solving the Maxwell equations in the frequency domain.

The surface as well as plasma reactions are specified in the chemistry module. Indeed, this part is most crucial to the reliability of the simulator. In the subsequent two sections, the reactions considered in this research are described for the bulk phase plasma, the wafer surface, and other walls.

3. Gas Phase Reactions

Due to the light mass, electrons are easily accelerated by electric field while ions are not. The average electron energy reaches 2-7 eV in a typical ICP etcher, which roughly corresponds to 20,000-80,000 K. On the other hand, the average ion energy remains around 0.03-0.06 eV or 350-700 K. Under such a non-thermal equilibrium state, plasma reactions are governed by the electron collision with neutral and ionic species. Reactions between heavy particles are scarce compared to the electron-impact reactions.

For an electron-impact reaction, the most fundamental information is the collision cross-section of the reaction. Fig. 3 shows the cross-section as a function of the electron energy for different electron-impact reactions of C_2F_6 gas. CFD-ACE+ is a continuum model-based program and the Arrhenius-type reaction rates are used instead of the cross-section data. For C_2F_6 plasmas, Arrhenius-type reaction rates of 132 gas phase plasma reactions are provided in CHEMKIN, a commercial program for reactor simulation [Meeks and Ho, 2000], by converting the cross-section data of Christophorou et al. [1998].

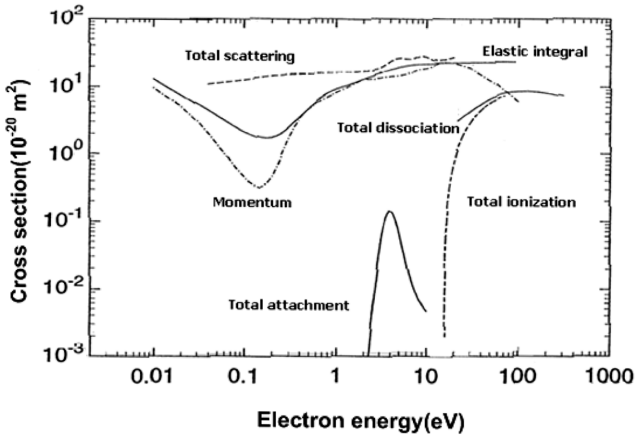

Fig. 3. Electron interaction cross sections for C_2F_6 gas [Christophorou et al., 1998].

Table 1. Gas-phase reactions for C_2F_6 plasmas (Reaction rate coefficients $k=AT_e^B\exp(-C/T_e)$, units: kmol, meter, seconds, and Kelvin)

Reaction	A	B	C
Ionization & Dissociation			
$C_2F_6+e\rightarrow 2CF_3+e$	7.99881×10^{-14}	0.10033	13.7131
$C_2F_6+e\rightarrow CF_3+CF_3^++2e$	9.28898×10^{-15}	0.87904	14.106
$C_2F_6+e\rightarrow CF^++CF^++2e$	1.08688×10^{-15}	0.86553	20.7527
$C_2F_6+e\rightarrow CF_4+CF^++F+2e$	1.00003×10^{-15}	1.0093	17.0386
$CF_4+e\rightarrow CF_3+F+e$	2.48222×10^{-17}	1.3087	12.4653
$CF_4+e\rightarrow CF_3+F^++e$	9.58009×10^{-16}	0.9375	34.6649
$CF_4+e\rightarrow CF_2+2F+e$	5.06791×10^{-18}	1.1844	14.3309
$CF_4+e\rightarrow CF_3^++F+2e$	1.48377×10^{-14}	0.76448	17.1756
$CF_4+e\rightarrow CF_3^++F^++3e$	1.99544×10^{-17}	1.4127	34.1814
$CF_4+e\rightarrow CF_2^++2F+2e$	3.43838×10^{-15}	0.51007	22.8287
$CF_4+e\rightarrow CF_2^++F^++F+3e$	1.37927×10^{-18}	2.4313	33.7092
$CF_3+e\rightarrow CF_3^++2e$	6.03125×10^{-15}	0.6481	9.76366
$CF_3+e\rightarrow CF_2+F+e$	6.24916×10^{-14}	−0.9407	11.2114
$CF_3+e\rightarrow CF_2+F^++2e$	8.38792×10^{-15}	0.28955	28.7438
$CF_3+e\rightarrow CF_2^++F+2e$	8.20373×10^{-15}	0.43666	17.1239
$CF_3+e\rightarrow CF^++2F+2e$	5.70236×10^{-15}	0.50598	21.1543
$CF_2+e\rightarrow CF+F+e$	2.48222×10^{-17}	1.3087	12.4653
$CF_2+e\rightarrow CF^++F+2e$	3.64391×10^{-15}	0.7803	13.8044
$CF_2+e\rightarrow CF_2^++2e$	5.67046×10^{-15}	0.62866	9.69558
$CF_2+e\rightarrow CF+F^++2e$	1.77025×10^{-14}	0.25189	38.3178
$CF+e\rightarrow CF^++2e$	2.10287×10^{-15}	1.038	8.8502
$F+e\rightarrow F^++2e$	2.33354×10^{-15}	0.85951	17.5987
Recombination			
$CF_2^++e\rightarrow CF+F$	4.0×10^{-14}	0	0
$CF_3^++e\rightarrow CF_2+F$	4.0×10^{-14}	0	0

Since that number is too large to accommodate in the two-dimensional rigorous ICP etcher model, we selected 24 reactions that have more direct effects on the SiO_2 etching. For example, electron-impact reactions with SiF_x gases that produce SiF_y gases and F radical were not included, since F is known to have far less effect on SiO_2 etching compared to CF_x radicals and ions. Likewise, electron-impact reactions with oxygen and CO were not considered. In Table 1, the reaction set considered in this research is shown. Indeed, it is the whole collection of the electron-impact reactions with all possible CF_x neutral and ionic components gathered in CHEMKIN.

4. Surface Reactions

The etching reactions on the SiO_2 surface are more difficult to investigate than the bulk phase plasma reactions since other hardly observable and measurable physical processes such as adsorption, surface migration, and desorption occur along with the reactions on the surface. Nonetheless, intensive researches during the past decade have enabled us to comprehend the overview and some key features of the surface reactions.

It was mentioned in the introduction that fluorocarbon plasmas are subject to competitive reactions between polymerization and etching on the SiO_2 surface. The CF_x and F radicals isotropically diffuse to and stick on the oxide surface to form 'surface sites' as monomer-covered oxide ($SiO_2CF_x^*$) and fluorinated oxide ($SiO_2F_2^*$). It is generally accepted that CF has the highest sticking tendency

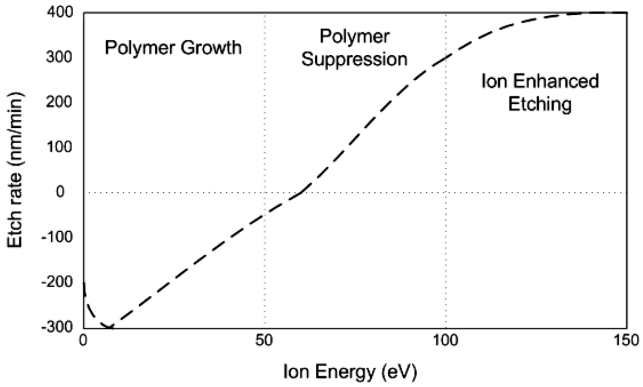

Fig. 4. Dominant surface reactions on SiO_2 with ion energy [Feldsien et al., 2000].

among CF_x and F radicals [Feldsien et al., 2000]. The active sites are easily combined with incoming radicals to form a polymer passivation layer with an F/C ratio of about one.

Unlike the radicals, ions are accelerated by the electric field over the plasma sheath and bombard the wafer surface in the vertical direction. The bombardment energy can be adjusted by the chuck bias voltage. Fig. 4 shows a typical trend on how the dominant surface reaction varies with the ion energy. At low ion energy (<50 eV), the ion bombardment cannot suppress the polymerization reaction. As the ion energy increases, ion bombardment overwhelms the polymerization by sputtering the polymer sites and removing the deposited polymer before it forms a continuous film [Oehrlein et al., 1994]. At even higher ion energy, the ions are actively reacting with SiO_2 together with other activated monomer sites to produce the etch products SiF_2 and SiF_4 with byproducts like CO and CO_2. The etch rate is significantly enhanced by the existence of activated monomer sites, and thus the ion enhanced etching (RIE) is enabled. Fluorine atom can directly etch the SiO_2 film but the contribution is not high compared to the ion reactions.

Even with the above-mentioned understanding, many features of the surface reactions still remain unexplained and quantitative description is still far from reality although the gap has been continuously reduced. In CFD-ACE+, the rate of the surface reaction is defined by the sticking coefficient. However, the sputtering yield is additionally considered in the ion enhanced reaction. For example, the rate of the radical reaction

$$F + 0.5\ SiO_2^*(S) \rightarrow 0.5\ SiO_2F_2^*(S) \quad (6)$$

Table 2. Surface reactions and sticking coefficients

Wafer	Sticking coefficients
$F + 0.25SiO_2(B) \rightarrow 0.25SiF_4 + 0.25O_2$	0.15823, E/R=1890
$F^+ + SiO_2^*(S) \rightarrow F + SiO_2^*(S)$	0.8
$F + 0.5SiO_2^*(S) \rightarrow 0.5SiO_2F_2^*(S)$	0.02
$F^+ + 0.5SiO_2^*(S) \rightarrow 0.5SiO_2F_2^*(S)$	0.2
$CF + SiO_2^*(S) \rightarrow SiO_2CF^*(S)$	0.66
$CF^+ + SiO_2^*(S) \rightarrow CF + SiO_2^*(S)$	0.8
$F + 0.5SiO_2CF^*(S) \rightarrow 0.5CF_3 + 0.5SiO_2^*(S)$	0.01
$CF^+ + SiO_2^*(S) \rightarrow SiO_2CF^*(S)$	0.2
$CF_2^+ + SiO_2^*(S) \rightarrow CF_2 + SiO_2^*(S)$	0.8
$CF_3^+ + SiO_2^*(S) \rightarrow CF_3 + SiO_2^*(S)$	0.8
$CF_3^+ + SiO_2(B) + 2SiO_2F_2^*(S) \rightarrow CF_3 + SiF_4 + O_2 + 2SiO_2(S)$	1
$CF_2^+ + SiO_2(B) + 2SiO_2F_2^*(S) \rightarrow CF_2 + SiF_4 + O_2 + 2SiO_2(S)$	1
$CF^+ + SiO_2(B) + 2SiO_2F_2^*(S) \rightarrow CF + SiF_4 + O_2 + 2SiO_2(S)$	1
$F^+ + SiO_2(B) + 2SiO_2F_2^*(S) \rightarrow F + SiF_4 + O_2 + 2SiO_2(S)$	1
$CF_3^+ + SiO_2(B) + 2SiO_2CF^*(S) \rightarrow CF_3 + SiF_2 + 2CO + 2SiO_2^*(S)$	1
$CF_2^+ + SiO_2(B) + 2SiO_2CF^*(S) \rightarrow CF_2 + SiF_2 + 2CO + 2SiO_2^*(S)$	1
$CF^+ + SiO_2(B) + 2SiO_2CF^*(S) \rightarrow CF + SiF_2 + 2CO + 2SiO_2^*(S)$	1
$F^+ + SiO_2(B) + 2SiO_2CF^*(S) \rightarrow F + SiF_2 + 2CO + 2SiO_2^*(S)$	1
$CF_2 + 1.5SiO_2^*(S) \rightarrow SiO_2CF^*(S) + 0.5SiO_2F_2^*(S)$	0.02
$CF_2^+ + 1.5SiO_2^*(S) \rightarrow SiO_2CF^*(S) + 0.5SiO_2F_2^*(S)$	0.2
Wall	
$CF_3^+ + e \rightarrow CF_3$	0.6
$CF_3^+ + e \rightarrow CF_2 + F$	0.4
$CF_2^+ + e \rightarrow CF_2$	0.7
$CF_2^+ + e \rightarrow CF + F$	0.28
$CF^+ + e \rightarrow CF$	1
$F^+ + e \rightarrow F$	1
$2F + M \rightarrow F_2 + M$	0.5
$2CF_3 \rightarrow C_2F_6$	0.01

is expressed as Sc [F][SiO_2^*(S)] where Sc, [F], and [SiO_2^*(S)] represent the sticking coefficient, volume concentration of F and surface concentration of the activated SiO_2 site, respectively. The rate of the ion enhanced reaction

$$CF_2^+ + ySiO_2(B) + 2ySiO_2F_2^*(S) \rightarrow CF_2 + yO_2 + y\,SiF_4 + 2ySiO_2^*(S) \quad (7)$$

is expressed as Sc [CF_2^+][SiO_2^*(S)]. Together with this, the sputtering yield is given as

$$y = \max[a(\sqrt{E_i} - \sqrt{E_{th}}), 0] \quad (8)$$

where E_i is the ion energy, and E_{th} is the threshold energy.

In this study, we relied on the reaction equations in CHEMKIN and selected 20 equations out of 55 for possible simulation in a reasonable time span. The selected reactions are the ones by CF_x and F ions and radicals while the deselected reactions included the ones by SiF_x, CO, CO, O, and O_2. The sticking coefficients were, however, partly modified so that the rate of the associated reactions complies with the experimental observations by other researchers [Mayer and Baker, 1982; Bell et al., 1994; Gray et al., 1993]. Since the reaction rates on polymerization are not contained in the CHEMKIN database, the simulation has been performed in the operating range where RIE prevails.

On the side wall, electrons are consumed by recombination reactions. We considered eight reactions by referring to CHEMKIN and the work by Feldsien et al. [2000]. In Table 2, surface reactions considered in this study are listed with sticking coefficients.

The surface reactions define the boundary conditions of the partial differential equations for the ICP model. For example, the boundary condition for the mass balance equation of species i is given by the following flux balance:

$$\mathbf{n} \cdot \mathbf{J}_i = S_i \quad (9)$$

where **n** is a unit normal vector to the surface and S is the surface production (or consumption) rate per unit area.

5. Feature Scale Simulation

Once CFD-ACE+ solves the ICP model, the energy and angle dependent distribution of each ion flux and the energy dependent distribution of each radical flux over the wafer surface are obtained. The radical fluxes are given angle-independent. CFD-TOPO inherits this information and calculates the time-varying etching profile using the level set method. CFD-TOPO has no parameters to tune except the initial geometry of the photo-resist pattern on the SiO_2 surface.

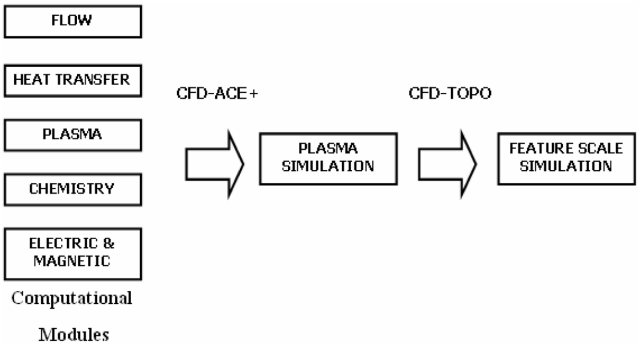

Fig. 5. CFD-ACE+/TOPO modules used for ICP etcher simulation.

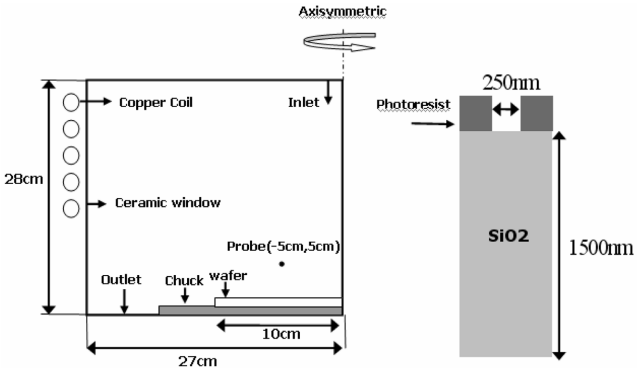

Fig. 6. Geometries of ICP etcher and wafer pattern considered in the two-dimensional simulation.

Incident angle dependent specular reflectivity data for each material on the wafer surface can be input by the user, but we used the default values that are provided in CFD-TOPO. Fig. 5 shows the overall structure of the ICP simulator by CFD-ACE+/TOPO.

SIMULATION STUDY

1. Chamber Geometry and Simulation Conditions

In Fig. 6, the detailed geometry of the ICP chamber model is shown together with the wafer pattern for feature scale simulation. Here, the point designated as 'probe' is the hypothetical position where plasma variables are measured. The RF coil is made of copper with radius of 0.6 cm and has five turns around the chamber wall. It is assumed that the chamber wall temperature is maintained at 300 K and the wafer temperature is regulated at 573 K. The wafer pattern is given as stripes with 250 nm of opening. The photo resist is assumed to be completely intact by the plasmas.

During the simulation study, C_2F_6 flow rate was fixed at 50 sccm since its effect is less salient than others once it exceeds a certain value. Consequently, the chamber pressure, main RF power, and bias voltage were chosen as the operating variables. We took the base condition of the operating variables as 10 mtorr, 2 kW, and 200 V and. By changing them over 5-30 mtorr, 150-300 V, and 1-3 kW around the base condition, the plasma as well as etching states were investigated and a linear regression model between the operating variables and etching state was determined for run-to-run con- troller design.

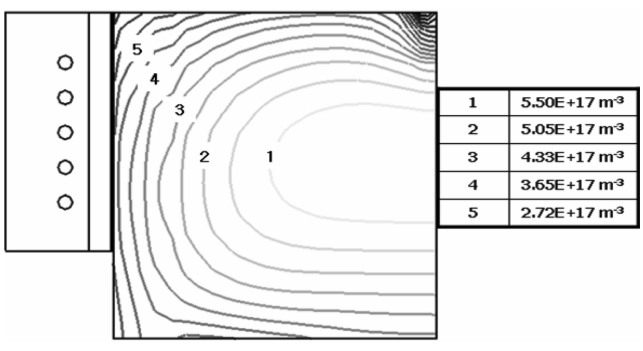

Fig. 7. Distribution of electron number density in the bulk plasma (2 kW, 10 mtorr, RF bias 200 V, 50 sccm C_2F_6).

2. Results and Discussion

Fig. 7 shows the distribution of the electron number density (END) in the chamber at the base condition. The simulator produced the maximum electron number density of 5.71×10^{17} m^{-3} and average electron temperature of 3.38 eV. These values correspond to the results in typical ICP [Kono et al., 2002; Sun et al., 2003; Efremov et al., 2004]. Since the recombination reactions that consume electrons mainly occur on the side wall, the electron number density is large at the plasma core and decreases gradually along the outward direction. Though not shown here, the number density and distribution of CF_x radicals were also found to agree well with the results by other researchers [Cunge and Booth, 1999; Hebner, 2002].

Fig. 8 shows the effects of operating variables on END at the probing position. The END increases with both RF power and pressure. Indeed, this is an expected result since the increase in the RF power and chamber pressure boosts the collision frequency by enhancing the electron energy and reducing the mean free path. On the other hand, the RF bias has little effect on the END, which is also expected. Although not shown here, the ion flux over the wafer surface shows the same trend with the operating variables as the END does. However, the radical flux decreases with the RF power.

In Fig. 9, the effects of the RF power and chamber pressure on the electron temperature (in terms of eV) at the probing position are depicted. Electrons gain energy from the RF power. Hence, the electron temperature increases with the RF power. On the other hand, the electron temperature is reduced by the decrease in the mean free path when the chamber pressure is increased.

Fig. 10 shows the angle-dependent distribution of CF^+ ion incident upon the wafer surface when 2 kW of RF power, 10 mtorr of pressure, and 200 V of RF bias were applied. The data were taken at the center position but similar results were obtained at other po-

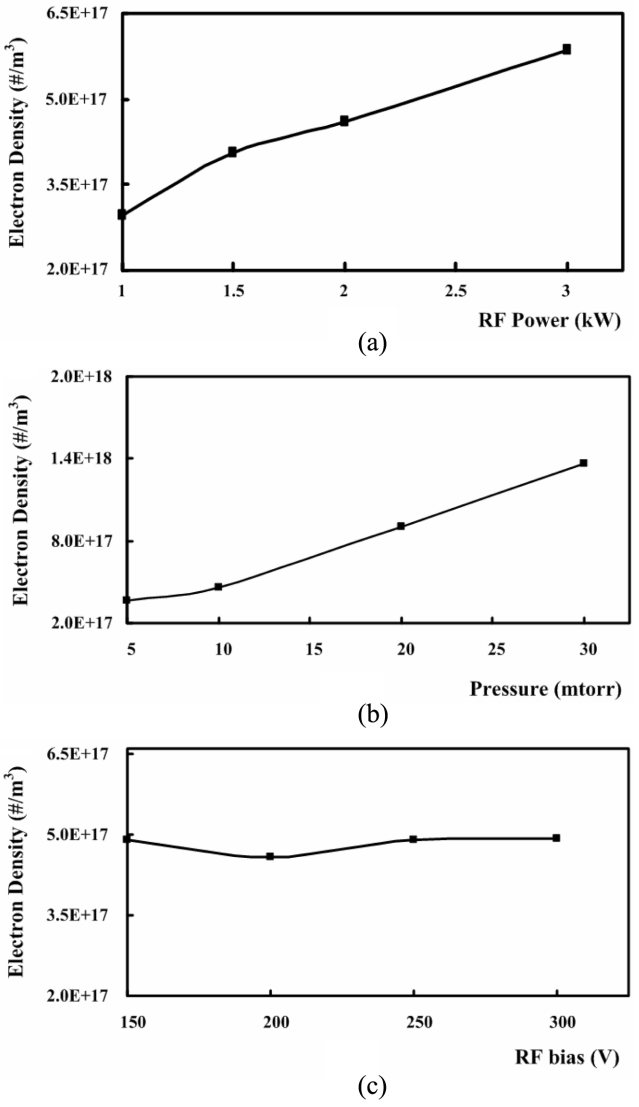

Fig. 8. Variation of electron density with changes in operating variables (probe position, 2 kW, 10 mtorr, RF bias 200 V, 50 sccm C_2F_6).

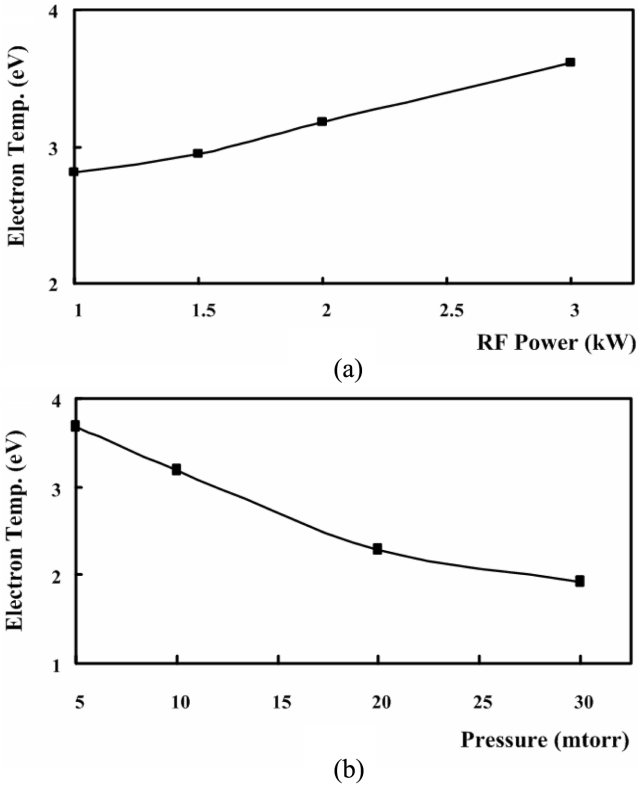

Fig. 9. Variation of electron temperature with (a) RF power and (b) pressure (probe position, 2 kW, 10 mtorr, 200 V RF bias, 50 sccm C_2F_6).

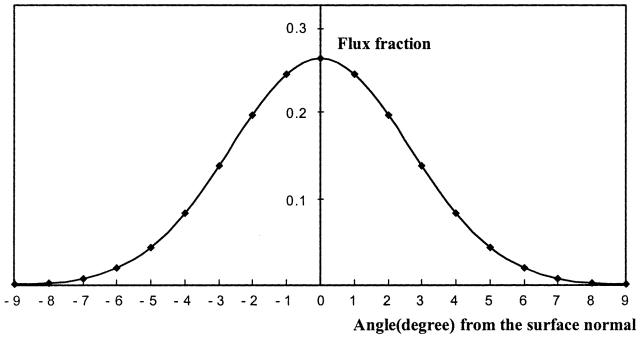

Fig. 10. Angle-dependent distribution of CF^+ ion incident on the wafer surface.

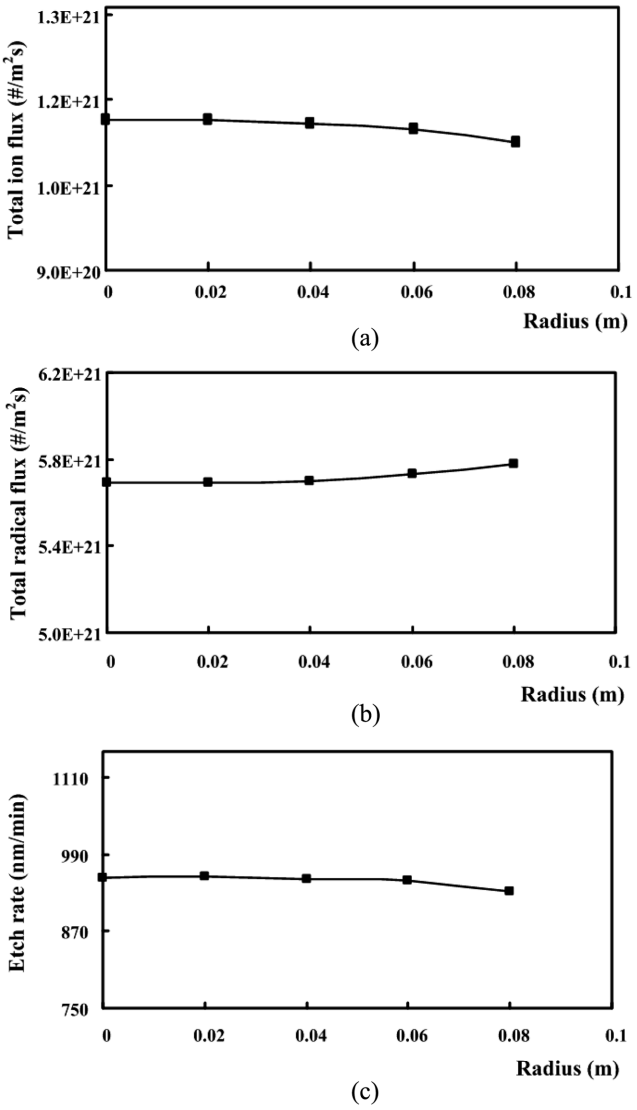

Fig. 11. Radial distributions of total ion flux, total radical flux, and etch rate (2 kW, 10 mtorr, 200 V RF bias, 50 sccm C_2F_6).

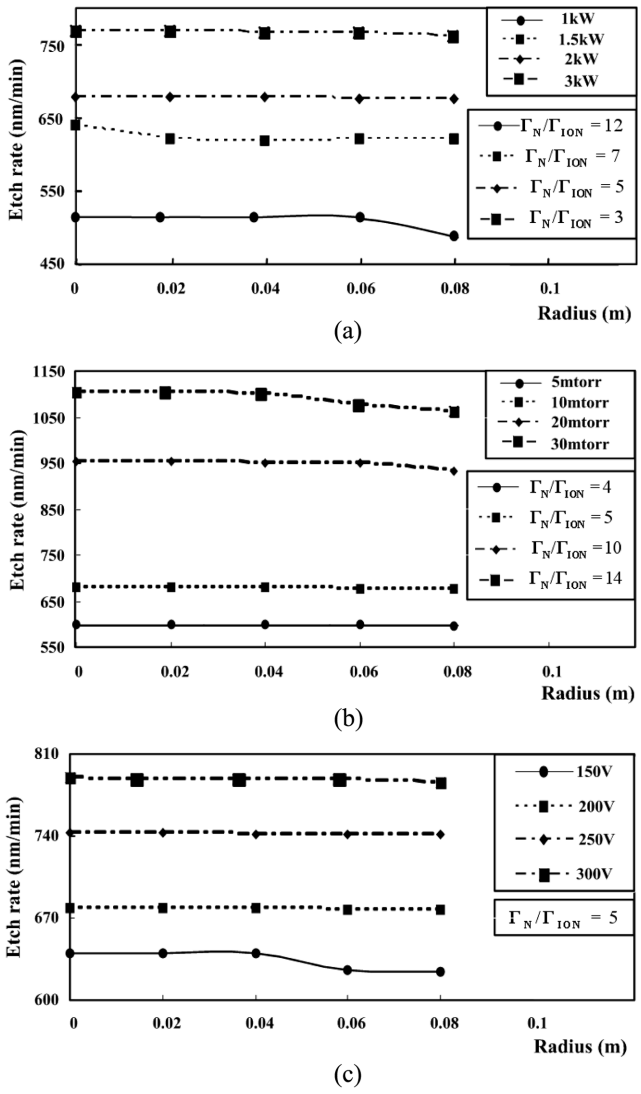

Fig. 12. Radial distribution of etch rate and radical to ion flux ratio with changes in (a) RF power, (b) pressure, and (c) RF bias (2 kW, 10 mtorr, 200 V RF bias, 50 sccm C_2F_6).

sitions, too. It can be seen that the ions attack the wafer at different angles but within 9 degrees from the surface normal. The distributions for other ionic species are not shown but only slightly different from that of CF^+.

Fig. 11 shows the profiles of the total ion flux, total radical flux, and etch rate at five radial points on the wafer surface. It can be seen that the radical flux tends to be higher at the wafer edge than at the wafer center, whereas the ion flux shows a reverse pattern. The reason for this is thought to be the recombination reactions on the wall, which consume ions and produce radicals. The etch rate decreases along the radial position but only slightly. It was mentioned that the radicals and ions enhance the etch rate in a synergic way through ion bombardment of activated monomer sites. Hence, the opposite pattern of the flux profiles gives a flattening effect on the etch rate profile.

Fig. 12 shows how the etch rate and uniformity vary with the change in the RF power, chamber pressure, and RF bias. Together with this, variation of the radical to ion flux ratio is shown. As can be seen from the figure, the etch rate increases monotonically with all three operating variables. The result is expected for the RF power and RF bias but not for the chamber pressure. Indeed, the effect of the chamber pressure is not easy to predict. At low pressure, increasing the chamber pressure offers the electrons higher collision frequency with the neural gas. The consequence is that more ions are produced and the etch rate is increased. At high pressure above a certain value, the mean free path becomes too short for the electrons to gain enough energy for ionization reaction. Under this situation, only the recombination reaction of the ions with the electrons can be enhanced and the ion concentration can be reduced. From the result in Fig. 12(b), we can see that 30 mtorr is not high enough for the recombination to prevail over the ionization for the concerned plasma etcher.

As for uniformity, however, the operating variables except the chamber pressure don not seem to yield outstanding trends. It can be seen that the uniformity deteriorates with an increase in the chamber pressure, whereas the other variables fail to show any distinct trend.

The radical to ion flux ratio (Γ_n/Γ_{ion}) was estimated to increase

with the RF power but decrease with the pressure. Since ionization requires higher energy than dissociation, more ions are produced as the RF power increases. With the pressure increase, however, the electrons cannot gain enough energy due to the reduced mean free path and the ion flux decreases in relation to the radical flux.

3. Linear Modeling

For future run-to-run controller design, a linear static model that relates the operating variables to the etch rate and uniformity was determined through linear regression. For this, a simulation was conducted at 64 different operating conditions. The etch rate was defined as the average value and the uniformity was defined as the normalized standard deviation over the five monitoring points, which is actually non-uniformity, such that

$$X(\text{nm/min})=(x1+x2+x3+x4+x5)/5 \tag{10}$$

$$NU(\%)=\frac{\sigma}{X}\times 100,$$
$$\sigma=\sqrt{\frac{(X-x1)^2+(X-x2)^2+(X-x3)^2+(X-x4)^2+(X-x5)^2}{4}} \tag{11}$$

Using the weighted least squares method, we obtained the following linear regression model:

$$\begin{bmatrix} X(\text{nm/min}) \\ NU(\%) \end{bmatrix}=\begin{bmatrix} 193.3632 & 20.1555 & 1.3352 \\ -0.3232 & 0.0460 & -0.0015 \end{bmatrix}\begin{bmatrix} \text{RF power(kW)} \\ \text{Pressure(mtorr)} \\ \text{RF bias(V)} \end{bmatrix}+\begin{bmatrix} -195.1989 \\ 1.2464 \end{bmatrix} \tag{12}$$

CONCLUSIONS

A numerical process to simulate SiO_2 etching with inductively coupled C_2F_6 plasmas was developed by using CFD-ACE+/TOPO. First, it was confirmed that the simulator provides reasonable results in terms of the number density and distribution of electron and radicals. Through extensive simulation study, it was observed that the etch rate and uniformity depend on both ion and radical fluxes on the wafer surface. Also, both fluxes were observed to be affected by RF power and chamber pressure, and the ion energy was shown to be strongly influenced by RF bias. From the above observations, the relation of RF power, chamber pressure, and RF bias to etch rate and uniformity was modeled through linear regression for future construction of a run-to-run control system.

ACKNOWLEDGMENTS

This work was supported by grant No. R01-2002-000-00574-0 from the Basic Research Program of the Korea Science & Engineering Foundation.

REFERENCES

An, K. J., Kim, H. S., Yoo, J. B. and Yeom, G. Y., "A Study on the Characteristics of Inductively Coupled Plasma using Multidipole Magnets and its Application to Oxide Etching," *Thin Solid Films*, **341**, 176 (1999).

Bell, F. H., Joubert, O., Oehrlein, G. S., Zhang, Y. and Vender, D., "Investigation of Selective SiO_2-to-Si Etching in an Inductively Coupled High-density Plasma using Fluorocarbon Gases," *J. Vac. Sci. Technol. A*, **12**, 3095 (1994).

Booth, J. P., Hancock, G., Perry, N. D. and Toogood, M. J., "Spatially and Temporally Resolved Laser-induced Fluorescence Measurements of CF_2 and CF Radicals in a CF_4 rf Plasma," *J. Appl. Phys.*, **66**, 5251 (1989).

Christophorou, L. G., Olthoff, J. K. and Rao, M. V., "Electron Interactions with C_2F_6," *J. Phy. Chem. Ref. Data*, **27**, 1 (1998).

Cunge, G. and Booth, J. P., "CF_2 Production and Loss Mechanisms in Fluorocarbon Discharges: Fluorine-poor Conditions and Polymerization," *J. Appl. Phy.*, **85**, 3952 (1999).

Efremov, A. M., Kim, D. P., Kim, K. T. and Kim, C. I., "Etching Characteristics and Mechanism of Pb(Zr,Ti)O_3 Thin Films in CF_4/Ar Inductively Coupled Plasma," *Vacuum*, **75**, 321 (2004).

Feldsien, J., Kim, D. S. and Economou, D. J., "SiO_2 Etching in Inductively Coupled C_2F_6 Plasmas: Surface Chemistry and Two-dimensional Simulation," *Thin Solid Film*, **374**, 311 (2000).

Gray, D. C., Tepermeister, I. and Sawin, H. H., "Phenomenological Modeling of Ion-enhanced Surface Kinetics in Fluorine-based Plasma Etching," *J. Vac. Sci. Technol B*, **11**, 1243 (1993).

Hebner, G. A., "Spatially Resolved CF, CF_2, SiF and SiF_2 Densities in Fluorocarbon Containing Inductively Driven Discharges," *Appl. Surface. Sci.*, **192**, 161 (2002).

Kim, W. C., Chin, I. S., Lee, K. S. and Choi, J. H., "Analysis and Reduced-order Design of Quadratic Criterion-based Iterative Learning Control using Singular Value Decomposition," *Comp. & Chem. Eng.*, **24**, 1815 (2000).

Kono, A., Konishi, M. and Kato, K., "Behaviors of Electron and Negative Ion Densities in Low-pressure High Density Inductively Coupled Plasmas of SF_6, NF_3, CF_4 and C_4F_6 Gases Diluted with Ar," *Thin Solid Films*, **407**, 198 (2000).

Lieberman, M. A. and Lichtenberg, A. J., *Principles of Plasma Discharges and Materials Processing*, John Wiley, New York, NY (1994).

Mayer, T. M. and Baker, R. A., "Reactive Ion Beam Etching with CF_4: Characterization of a Kaufman Ion Source and Details of SiO_2 Etching," *J. Electrochem. Soc.*, **129**, 585 (1982).

Meeks, E. and Ho, P., "Modeling Plasma Chemistry for Microelectronics Manufacturing," *Thin Solid Film*, **365**, 334 (2000).

Oehrlein, G. S., Zhang, Y., Vender, D. and Joubert, O., "Fluorocarbon High-density Plasmas. II. Silicon Dioxide and Silicon Etching using CF_4 and CHF_3," *J. Vac. Sci. Technol. A*, **12**, 333 (1994).

Qi, S., Lifang, X., Xinxin, M. and Mingren, S. M., "Effect of Plasma Density on the Distribution of Incident Ions and Depth Profile in Plasma-based Ion Implanted Layers," *Appl. Sur. Sci.*, **206**, 53 (2003).

Rolland, L., Peignon, M. C., Cardinaud, Ch. and Turban, G., "SiO_2/Si Selectivity in High Density CHF_3/CH_4 Plasmas: Role of the Fluorocarbon Layer," *Microelectronic Eng.*, **53**, 375 (2000).

Thomas, J. W., Suzuki, J. R., Kable, S. H. and Steinfeld, J. I., "Laser-induced Fluorescence Measurement and Analytical Model for the Reaction Probability of CF_2 on Si," *J. Appl. Phys.*, **60**, 2775 (1986).

Tserepi, A. D., Derouard, J., Booth, J. P. and Sadeghi, N., "CF_2 Kinetics and Related Mechanisms in the Presence of Polymers in Fluorocarbon Plasmas," *J. Appl. Phys.*, **66**, 2124 (1997).

Xiao, H., *Introduction to Semiconductor Manufacturing Technology*, Prentice Hall, Upper Saddle River, New Jersey (2001).